

AD748328

1
D D C
RECORDED
SEP 18 1962
R
F K

THERMAL AND OPTICAL EMISSION RATES AND CROSS SECTIONS FROM THE IMPURITY PHOTOCURRENT AND PHOTOCAPACITANCE METHODS[†]

C. T. Sah*, L. Forbes*, L. L. Rosier ** and A. F. Tasch, Jr.^{**}

I. Introduction

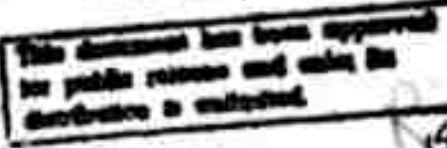
Electrical and optical properties of impurity centers in semiconductors such as energy level scheme, thermal and optical cross sections, and thermal emission rates have been measured and studied using the steady state and transient photoconductivity measurements, infrared absorption, Hall effect and conductivity over a wide range of temperatures, thermally stimulated conductivity and other methods.¹ These measurements are performed on uniform sample near thermal equilibrium where both emission and capture of electrons and holes at the center proceed at comparable rates. The nonlinearity and the carrier concentration dependences of the capture processes result in complex photoconductivity decay and large uncertainty in the cross section data. In this paper, several measurement techniques of these thermal and optical parameters using reverse biased p-n junctions are discussed which have simple exponential decays since the capture rates are negligible. Detailed measurements have been made on the gold acceptor and donor centers in silicon.

II. Thermal Emission Rates from Dark Junction Current and Capacitance Transients

The thermal emission rates of electrons and holes, e_n^t and e_p^t , from the impurity centers are obtained by either the dark junction capacitance or current transient or the photocurrent transient under square wave illumination discussed in IV.

The dark capacitance transient experiments were performed by recording the high-frequency small-signal capacitance of a P+N (p-side very heavily doped compared with n-side which has a spatially uniform impurity concentration of N_1) or N+P

* This research was supported in part by the Advanced Research Projects Agency under Contract SD-131 and in part by the Air Force Office of Scientific Research.



**BEST
AVAILABLE COPY**

diode after the junction voltage is switched from 0 to a large reverse bias $-V_R$. The capacitance rise with time after switching comes from the emission of the electrons at the impurity centers in the depletion region which were trapped when $V_R = 0$. This is given by

$$C^2(t) = qN_I(t)A^2/2K_s \epsilon_0 (V_D + V_R) \quad (1)$$

where K_s is the static dielectric constant of the semiconductor, $\epsilon_0 = 8.85 \times 10^{-14} \text{ F/cm}^2$, V_D is the junction barrier height at zero bias, V_R is the magnitude of the reverse bias, and A is the junction area.

The net ionized impurity concentration contains both the fixed shallow level donor of the n-type side and the trapped electrons at the deep-level impurity centers whose properties are to be determined. For a P+N junction, these are given by

$$\begin{aligned} N_I(t) &= N_D + p_T(t) && \text{donor-like center} \\ &= N_D - n_T(t) && \text{acceptor-like center} \end{aligned} \quad (2)$$

For N+P junction, the sign of the time dependent terms are changed. The trapped hole, $p_T(t)$, and electron, $n_T(t)$, concentrations are given by the solution of the linear kinetic equation $dn_T/dt = (e_n^t + e_p^t)n_T - e_p^t N_{TT}$ where $N_{TT} = n_T + p_T$ is the total deep level impurity concentration. The initial and final conditions are

$$n_T(0) = N_{TT}[N_E/(N_E + n_1)] \quad (3)$$

$$= N_{TT} \quad (\text{P+N junction}) \quad (3A)$$

$$= 0 \quad (\text{N+P junction}) \quad (3B)$$

and

$$n_T(\infty) = N_{TT}[e_p^t/(e_n^t + e_p^t)] \quad (4)$$

The solution for the trapped electron concentration is then

$$n_T(t) = n_T(\infty) + [n_T(0) - n_T(\infty)]\exp(-t/\tau_{ON}) \quad (5)$$

where $\tau_{ON} = 1/(e_n^t + e_p^t)$.

Thus, a measurement of the time constant gives directly the sum of the emission rates. Additional data of $C^2(0)$ and $C^2(\infty)$ and N_D from control sample would give N_{TT} [from $C^2(0)$ and N_D for a P+N junction] and the ratio e_n^t/e_p^t so that e_n^t and e_p^t can be individually determined.

The capacitance method is limited by the instrument response and is particularly useful at low temperatures where the thermal emission rates are long. Typical experimental data of a gold doped silicon P+N diode is shown in Fig. 1 (a) and (b) indicating the expected behavior and the true exponential response.

For higher temperatures when the junction current is sufficiently high, the emission rates can be determined from the waveform of the dark junction current transient during the switching from 0 to a large reverse bias $-V_R$. The junction current contains two component during the transient phase after switching from 0 to $-V_R$: the conduction and the displacement currents. These are given by

$$i_{cn}(t) = A \int_0^W q(dn/dt)_T dx = qe_n^t n_T(t) W(t) \quad n_T \neq f(x) \quad (6)$$

and

$$i_d(t) = A \int_0^W q(dn_T/dt)(x/W) dx = (qA/2)(dn_T/dt)W(t) \quad (7)$$

where W is the width of the transition region, $W = \sqrt{2K_s \epsilon_0 (V_D + V_R) / qN_I(t)}$, $(dn/dt)_T = e_n^t n_T$ is the electron emission rate from the center, dn_T/dt and n_T are given by (5). The two current components are evaluated at $x=W$. The total junction current is then

$$i(t) = (qWA/2)(e_p^t p_T + e_n^t n_T) \quad (8)$$

where $n_T(t) = N_{TT} - p_T(t)$ is given by (5). Thus, a measurement of the ratio

$$\begin{aligned} i(0)/i(\infty) &= (1/2)(1 + e_n^t/e_p^t)(W_0/W_\infty) && (\text{P+N junction}) \\ &= (1/2)(1 + e_p^t/e_n^t)(W_0/W_\infty) && (\text{N+P junction}) \end{aligned} \quad (9)$$

and the decay time constant $\tau_{ON} = 1/(e_n^t + e_p^t)$, would give e_n^t and e_p^t directly if W does not change appreciably with time or $W_0 \approx W_\infty$, when $N_{TT} \ll N_D$. If N_{TT} is comparable to N_D (or N_A), then a correction from W_0/W_∞ can be made using the capacitance data. A typical experimental data is given in Fig.2(a) and (b) showing slight departure from true exponential due to $W=W(t)$.

III. Optical Cross Sections from Photocapacitance and Photocurrent at Low Temperatures

The optical emission rates, e_n^0 and e_p^0 , and the optical cross sections, $e_n^0 = \sigma_n^0(\lambda\omega)\phi(\lambda\omega)$ and $e_p^0 = \sigma_p^0(\lambda\omega)\phi(\lambda\omega)$ where $\phi(\lambda\omega)$ is the monochromatic photon flux at $\lambda\omega$, can be obtained readily at low temperatures when the thermal emission rates are negligible. Under this low temperature condition, the results obtained for the high temperature dark capacitance and current transients given by (1) to (9) are all applicable here provided that e_n^t is replaced by e_n^0 and e_p^t is replaced by e_p^0 . The waveforms of both the $C^2(t)$ and $i(t)$ transients are identical except that an initial current spike in the dark current transient does not appear here.

An additional variable parameter in these photoexcitations, not available in the dark or thermal excitation in section II, is the wave length of light. For an deep level not exactly located at the midgap position, the photon energy can be varied so that either e_n^0 or e_p^0 is made zero. For example, take a P+N gold doped Si junction at 77°K. The acceptor level is located at $E_C - E_T = 0.54$ eV and $E_T - E_V = 0.62$ eV. Then with $\lambda\omega = 0.58$ eV, we have $e_n^0 > 0$ while $e_p^0 = 0$. Suppose that the junction is switched from 0 to $-V_R$ reverse bias at 77°K and then monochromatic light with 0.58 eV is direct to the junction. The junction capacitance would rise with a time constant of $\tau_{ON} = 1/e_n^0$ and the ratio of initial to final value is $[C(0)/C(\infty)]^2 = 1 - (N_{TT}/N_D)$ giving the ratio N_{TT}/N_D . As the photon energy is increased to $\lambda\omega > E_T - E_V$, e_p^0 becomes nonzero and $\tau_{ON} = 1/(e_n^0 + e_p^0)$. In addition, the capacitance

ratio becomes $[C(0)/C(\infty)]^2 = [1 - (N_{TT}/N_D)]/[1 - (N_{TT}/N_D)e_p^0/(e_p^0 + e_n^0)]$. Since N_{TT}/N_D was already determined at longer wavelength, both e_n^0 and e_p^0 can be determined. Explicitly, for an acceptor level located above midgap such as gold in Si, we have

$$(e_p^0/e_n^0)_{\lambda} = [C(0)/C(\infty)]_{\lambda}^2 - [C(0)/C(\infty)]_{\lambda+}^2 \quad (10)$$

where λ is the wavelength of light with $\lambda > E_T - E_V$ while $\lambda+$ is that with $E_C - E_T < \lambda < E_T - E_V$. A typical experimental data showing the feature just described is given in Fig. 3 where the 0.59 eV photoexcitation remove all the electrons trapped at the gold acceptor level, $E_C - E_T = 0.54$ eV, giving a capacitance change of $6.0 - 5.2 = 0.8$ pF while at a shorter wave length of 0.67 eV, photoemission-of-holes results in a steady state trapped electron concentration of $n_T(\infty)/N_{TT}$ $= e_p^0/(e_p^0 + e_n^0) = [6.0^2 - 5.63^2]/[6.0^2 - 5.2^2] = 1/2.1$ so that $e_n^0/e_p^0 = 1.1$ at 0.67 eV.

IV. Optical and Thermal Emission Rates from Photocapacitance and Photocurrent at High Temperatures

Three type of initial conditions for the trapped charges, $n_T(0)$, can be employed in this most general case where both thermal and optical emissions must be included in analyzing the experimental data. These are: (1) the dark steady state, (2) the equilibrium and (3) band-impurity photoexcitation at two different intensity levels. (1) was previously proposed as the impurity photovoltaic effect,^{2/} (2) makes use of the same initial condition as in sections II and III and provides simplification and unique interpretation of results because of asymmetry between electrons and holes and (3) can be used to extend the light chopping rate to nanosecond speed using electro-optics techniques. We shall describe only the initial condition listed under (1). The others are discussed elsewhere.^{3/}

For the type (1) initial condition, we suppose that the on-duration of the square wave light is much longer than the rise time constant, $t_{(N=1)}^{(t)} / (e_n^{t0} + e_n^{t0} + e_p^{t0} + e_p^{t0})$, then during the turn-on transient by light with junction reverse bias $-V_R$ on at

all time, we have

$$n_T(0) = N_{TT} e_p^t / (e_n^t + e_p^t) \quad (11)$$

and

$$n_T(\infty) = N_{TT} [(e_p^t + e_p^0) / (e_n^t + e_n^0 + e_p^t + e_p^0)] \quad t_{ON} \gg \tau_{ON} \quad (12)$$

$n_T(t)$ is given by (5) with $\tau_{ON} = 1 / (e_n^t + e_n^0 + e_p^t + e_p^0)$. The turn-on transient.

The initial and final values of n_T during the turn-off phase, $t=0$, are just those given by (11) and (12) interchanged and $n_T(t)$ is still given by (5) but $\tau_{OFF} = 1 / (e_n^t + e_p^t)$.

The capacitance transients during turn-on phase will either rise or decay depending on the ratio of optical to thermal emission rates. For a P+N diode, the capacitance will: (1) rise if $(e_n^t / e_p^t) < (e_n^0 / e_p^0)$, (2) stay constant if $(e_n^t / e_p^t) = (e_n^0 / e_p^0)$ or (3) decay if $(e_n^t / e_p^t) > (e_n^0 / e_p^0)$. (1) and (3) are interchanged during the turn-off phase. The capacitance transients can be used to determine the sum of $e_n^t + e_p^t$ and $e_n^t + e_n^0 + e_p^t + e_p^0$ or $e_n^0 + e_p^0$ from the turn-on and turn-off time constants. In addition, a ratio of e_p^t / e_p^0 or e_n^t / e_n^0 can be determined if N_D (or N_A) and N_{TT} are determined from other experiments.

The photocurrent transient can be obtained directly from (8) using (5) and the initial and final values given by (11) and (12). If the thermal emission rates in (8) are replaced by the total emission rates, $e_n = e_n^t + e_n^0$ and $e_p = e_p^t + e_p^0$. The total current during the turn-on phase is given by

$$I_{ON}(t) = (qWA/2) [(e_p^t + e_p^0)p_T + (e_n^t + e_n^0)n_T] \\ = qWA N_{TT} \left\{ [e_n e_p / (e_n + e_p)] + \frac{1}{2} [(e_n^0 e_p^t - e_n^t e_p^0)(e_n - e_p) / (e_n^t + e_p^t)(e_n + e_p)] \exp(-t/\tau_{ON}) \right\}$$

for the case of constant W or low N_{TT} compared with N_p or N_A . This is also valid for arbitrary N_{TT} in a P+IN+ diode operated in the punch-through mode so that W is the width of the constant I-layer.

The turn-off phase current can be readily obtained in the same way and is obtained from (13) by interchanging $e_n^t + e_n^o$ or e_n with e_p^t and $e_p^t + e_p^o$ or e_p with e_p^t .

Due to the abrupt change of the emission rates at $t=0$ and $t=t_{ON}$ when the light is turned on and off, photocurrent steps are obtained and denoted by S_{ON} and S_{OFF} as indicated in Fig. 4. These are given by

$$S_{ON} = qAN_{TT}W(e_n^t e_p^o + e_n^o e_p^t)/2(e_n^t + e_p^t)$$

and

$$S_{OFF} = qAN_{TT}W(e_n^t e_p^o + e_n^o e_p^t + 2e_n^o e_p^o)/2(e_n^t + e_p^t)$$

(14)

The total photocurrent transient, excluding the initial step, are denoted by Δ_{ON} and Δ_{OFF} in Fig. 4. These are given by

$$\Delta_{ON} = -(qAN_{TT}W/2)(e_n^o e_p^t - e_n^t e_p^o)(e_n^t - e_p^t)/(e_n^t + e_p^t)(e_n^o + e_p^o)$$

and

$$\Delta_{OFF} = -(qAN_{TT}W/2)(e_n^o e_p^t - e_n^t e_p^o)(e_n^t - e_p^t)/(e_n^t + e_p^t)(e_n^o + e_p^o)$$

(15)

It can be readily shown that $|\Delta_{ON}/S_{ON}| < 1$ and $|\Delta_{OFF}/S_{OFF}| < 1$. This means that the initial steps of the turn-on and turn-off transients must be greater than one-half of the total steady state photocurrent: $S_{ON} \geq \Delta_{SS}/2$ and $S_{OFF} \geq \Delta_{SS}/2$.

Three shapes of the turn-on and turn-off phase transients are possible as illustrated in Fig. 4(c). They correspond to positive (+), zero (0) and negative (-) values of Δ_{ON} and Δ_{OFF} . Only six combinations of the turn-on and turn-off transient waveforms can exist which are $(ON, OFF) = (00), (0+), (-0), (++), (-+)$ and $(-+)$ as illustrated by the map shown in Fig. 4(d). In this map, the behavior of $C^2(t)$ corresponding to the three cases discussed previously is also indicated.

The measurements of τ_{ON} , τ_{OFF} , $S = S_{ON}/S_{OFF}$ and $\beta = \Delta_{ON}/\Delta_{OFF}$ can in principle provide enough information to determine all the four emission rates, e_n^t , e_p^t , e_n^o and e_p^o .

e_p^0 . However, an ambiguity arises due to the complete symmetry of the results with respect to electrons and holes and it is not possible to distinguish e_n^t from e_p^t nor e_n^0 from e_p^0 . However, a determination of the ratio e_n^0/e_p^0 by getting below the threshold of e_p^0 or e_n^0 or a determination of the ratio e_n^t/e_p^t from dark current transient described in section II will then allow a complete determination of all of the four emission rates unambiguously. It is noted that a knowledge of the impurity concentration, N_{TT} , is not required.

Typical results of the photocurrent transient showing the predicted features of current steps and either initial rise or decay after the step are given in Fig. 5. This was taken on a gold doped silicon PIN diode and the photoresponse comes from the gold acceptor level located at $E_C - E_Au = 0.54$ eV.

V. Experimental Results

Experimental results are obtained for the gold centers in silicon using the methods just described. The gold impurity has two energy levels in the band gap of silicon whose thermal activation energies are: acceptor level, $E_C - E_{Au} = 0.54$ eV and donor level, $E_{Au} - E_V = 0.35$ eV.^{4/} The thermal emission rates of electrons and holes at the acceptor level, e_n^t and e_p^t , and the thermal emission rate of holes at the donor level, e_{p-1}^t , are determined by the dark capacitance and current transients described in section II. These are graphed as solid dots and triangles in Fig. 6. The thermal rates at the acceptor level were also obtained from the high temperature photocurrent experiment described in IV and are shown as circles. e_{p-1}^t cannot be determined from the photocurrent experiment described since the donor level is inactive during the transient. The electron emission rate from the donor level, e_{no}^t , is too slow to be measured in all of these experiments.

Data from other experiments are also shown in Fig. 6. The pulsed field effect^{5/} data are shown as \ominus and the noise corner frequency data^{6/} is shown as Δ .

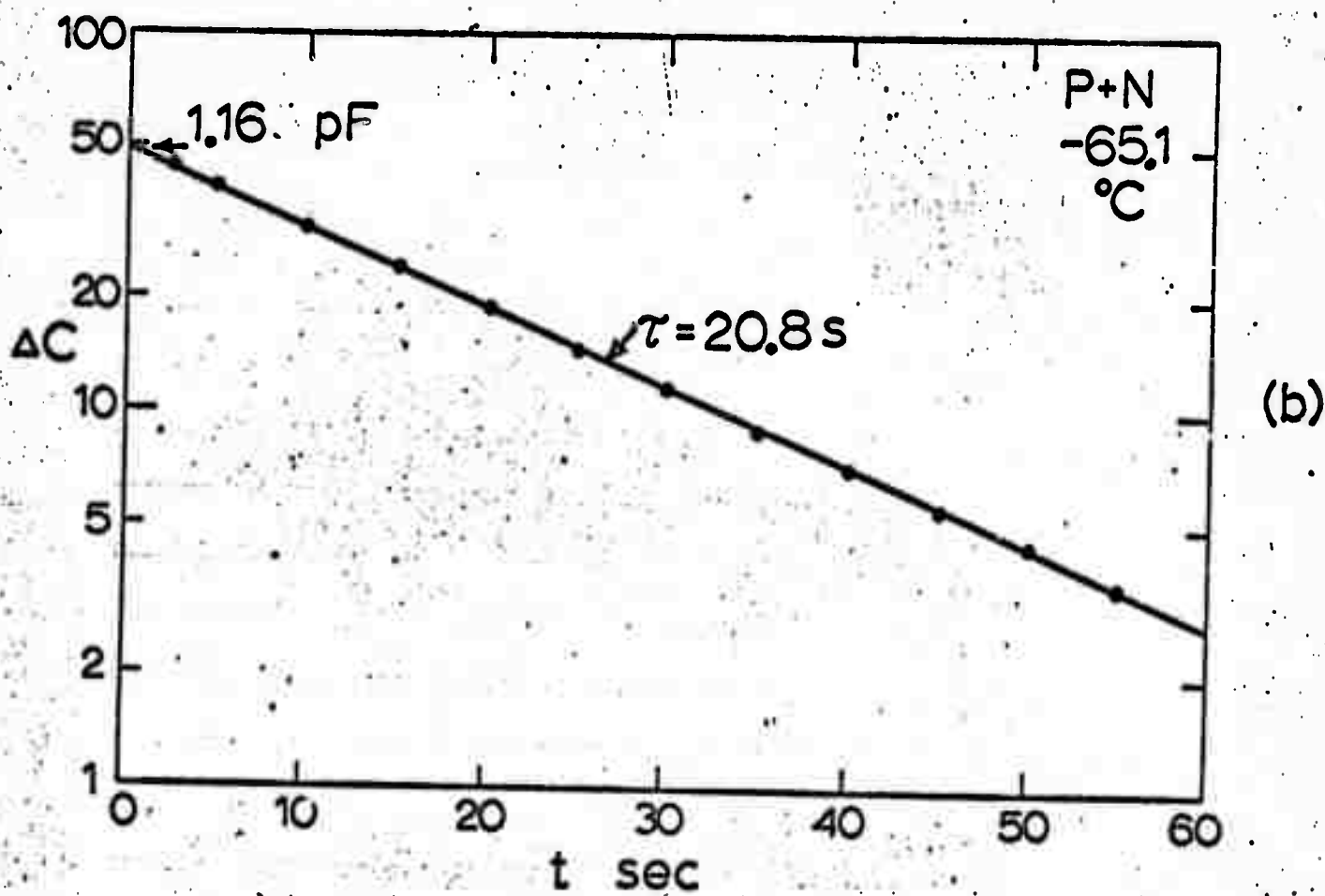
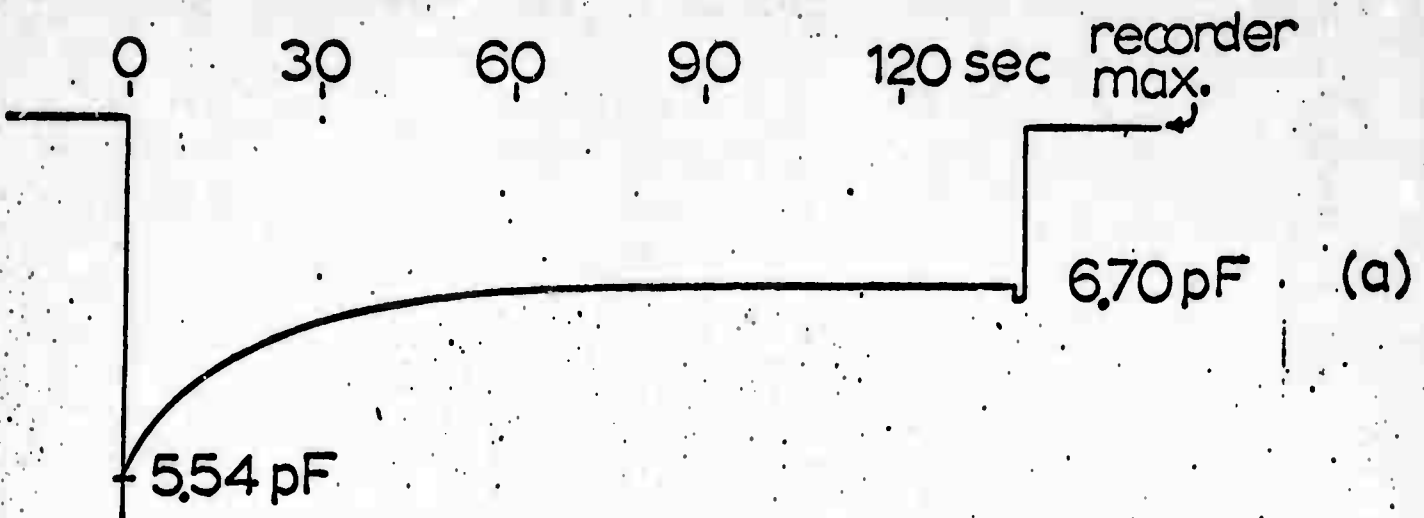
The optical cross sections are obtained from either the low temperature photocapacitance transient shown in section III or the photocurrent transient shown discussed in section IV. These are shown in Fig. 7. The data are taken at about 100°K and essentially independent of temperature as indicated by data at 188°K at 1.80 microns.

References

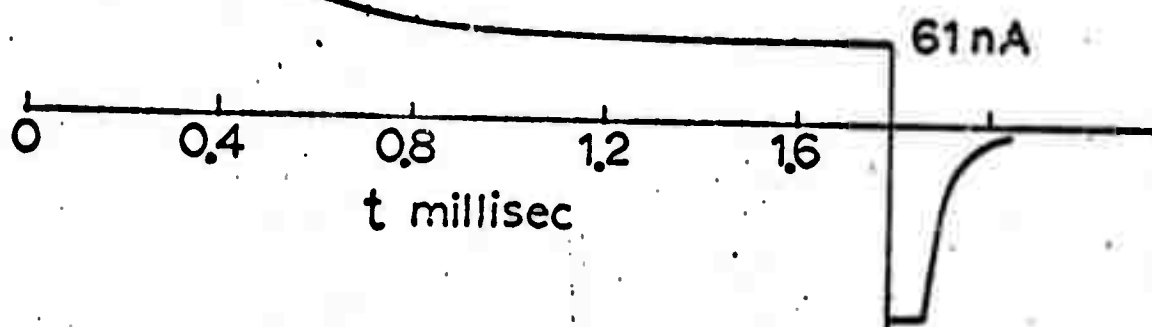
1. R. H. Bube, Photoconductivity of Solids, Wiley (1960)
2. C. T. Sah and A. F. Tasch, Jr. Phys. Rev. Letts 19, 69 (1967); C. T. Sah, A. F. Tasch, Jr. and D. K. Schroder, ibd. 71 (1967)
3. C. T. Sah, L. Forbes, L. L. Kosier and A. F. Tasch, Jr. to be published
4. C. B. Collins, R. O. Carlson and C. J. Gallagher, Phys. Rev. 105, 1168 (1957)
5. S. Sato and C. T. Sah, to be published
6. L. D. Yau and C. T. Sah, to be published

Caption of Figures

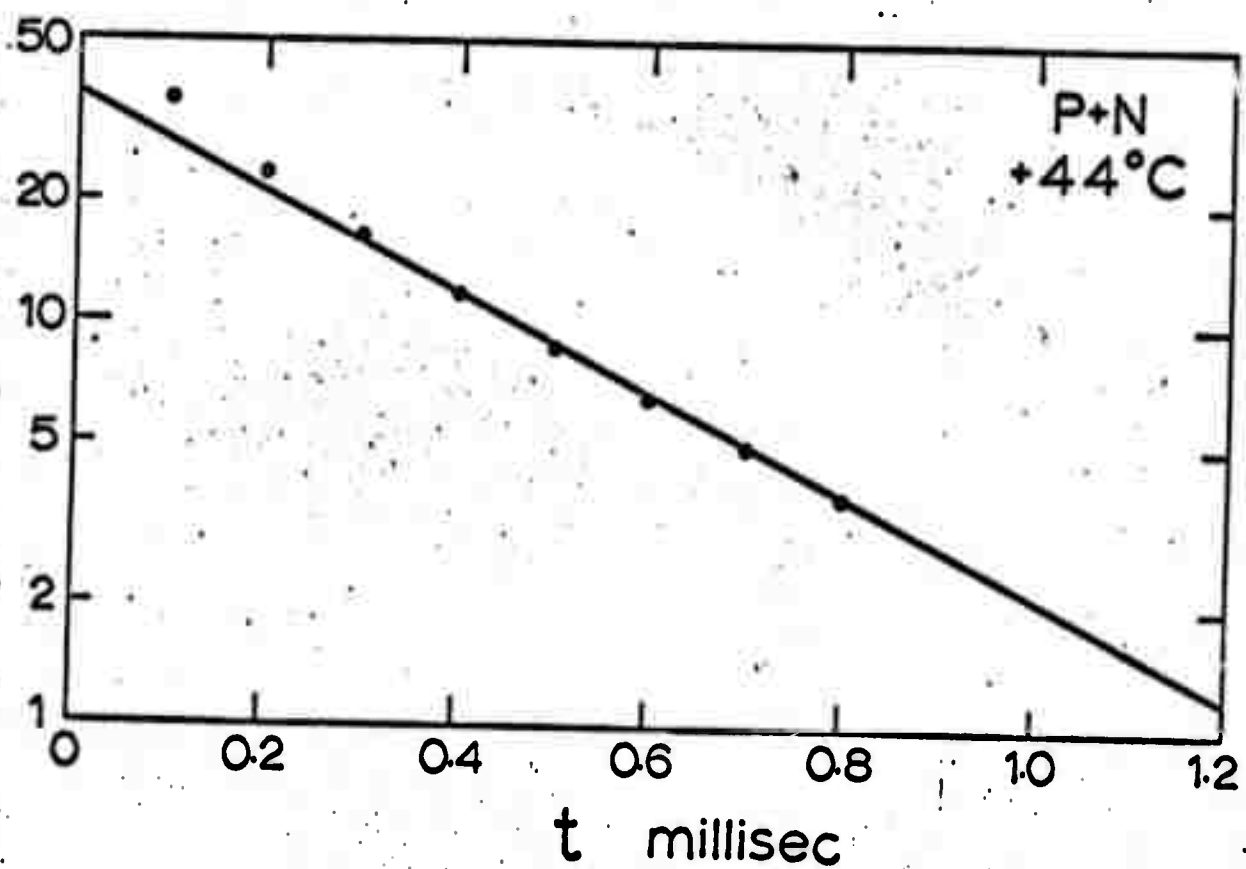
1. The dark capacitance transient waveform of a gold doped silicon P+N junction.
(a) x-y recorder trace and (b) AC vs time showing true exponential decay.
2. The dark current transient waveform of a gold doped silicon P+N junction.
(a) x-y recorder trace and (b) Δi vs time showing initial nonexponential decay due to $W=W(t)$.
3. Low temperature photocapacitance transient waveform at the gold acceptor center in a gold doped silicon P+N diode. Curve labeled 0.59 eV corresponds to optical excitation of electrons only while that of 0.67 eV contains both optical excitation of electrons and holes at the gold center of $E_C-E_V=0.54$ eV and $E_T-E_V=0.62$ eV.
4. The waveforms (a), (b) and (c) of the high temperature photocurrent transient with $V_R/V_R(t)$. Part.(d) shows that map relating the wave form in (c) to the ratios: e_n^t/e_p^t , e_p^0/e_p^t and e_n^0/e_n^t .
5. Examples of experimental traces of the photocurrent waveform due to the gold acceptor level in a silicon PIN diode.
6. Experimental data of emission rate vs temperature from experiments described in sections II and IV and from small signal pulsed field effect \ominus and from g-r noise data Δ .
7. Photoionization cross sections of electrons and holes at the gold acceptor center and gold donor center in silicon at about 100°K. The data of σ_{p-1}^0 of the gold donor level are obtained from the low temperature photocapacitance method described in section III and the data of σ_{p0}^0 and σ_{n1}^0 are obtained from the high temperature photocurrent method described in section IV.



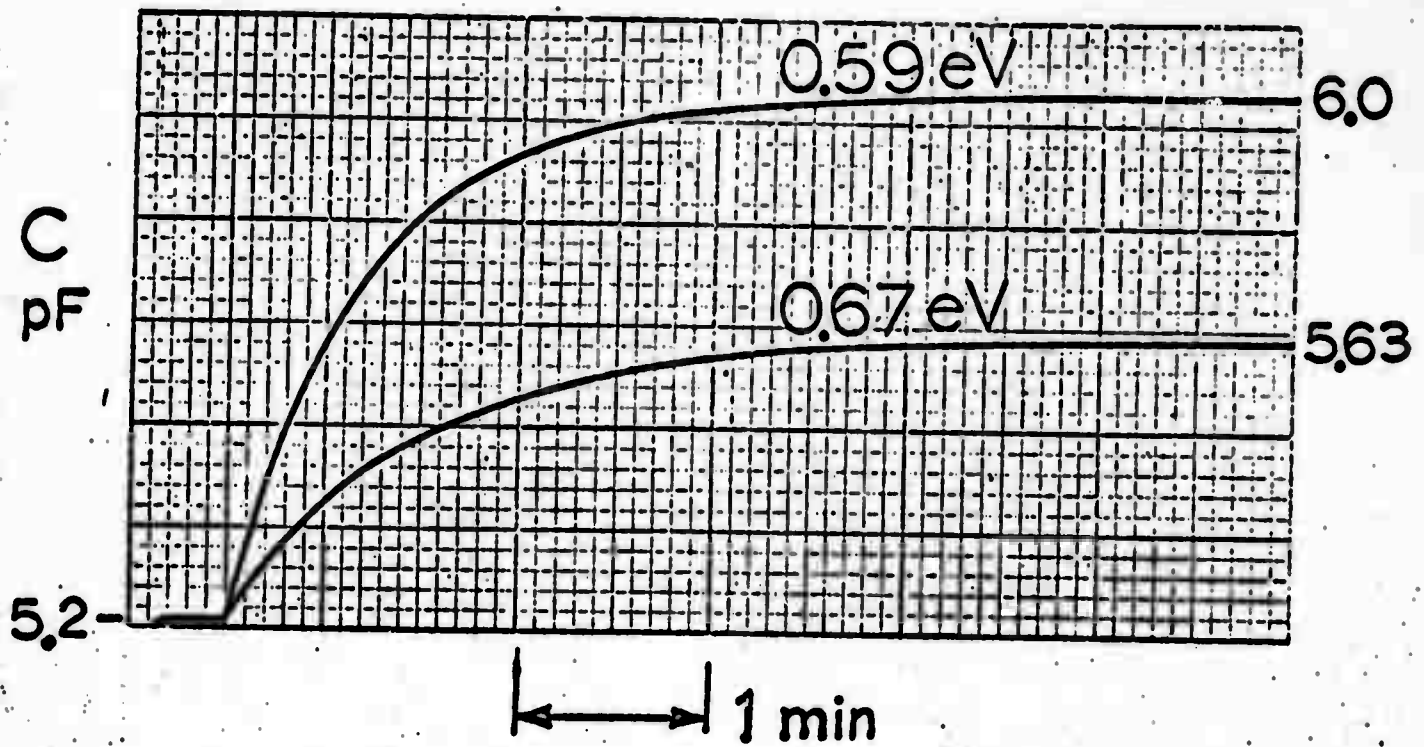
(a)



(b)

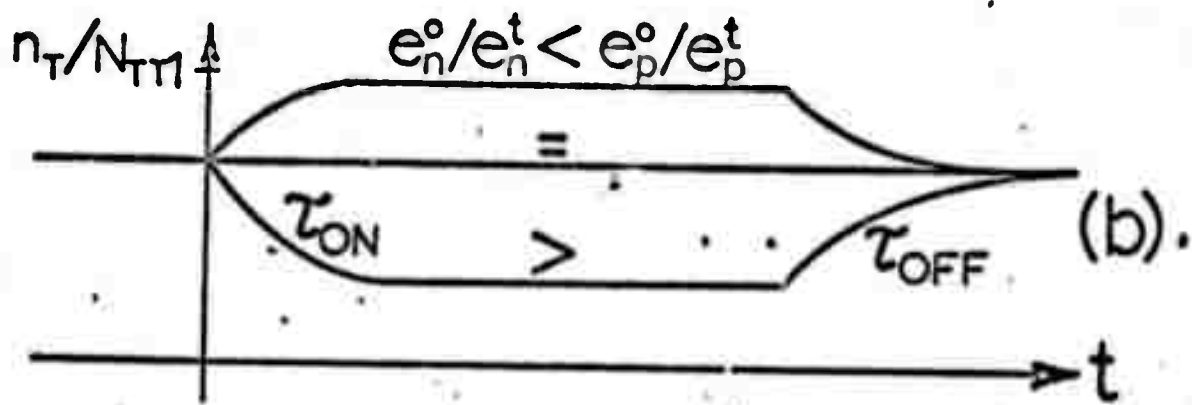
Fig. 2
Sah et al.

166°K

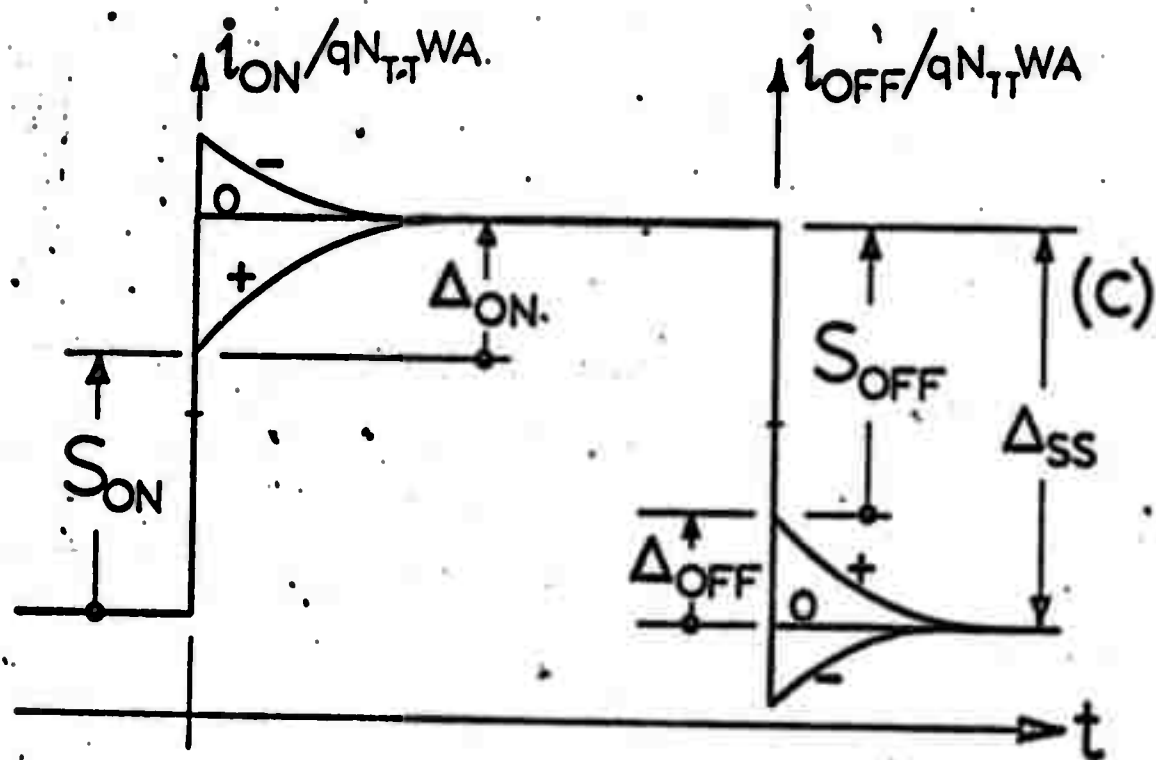


Sah et al Fig.3

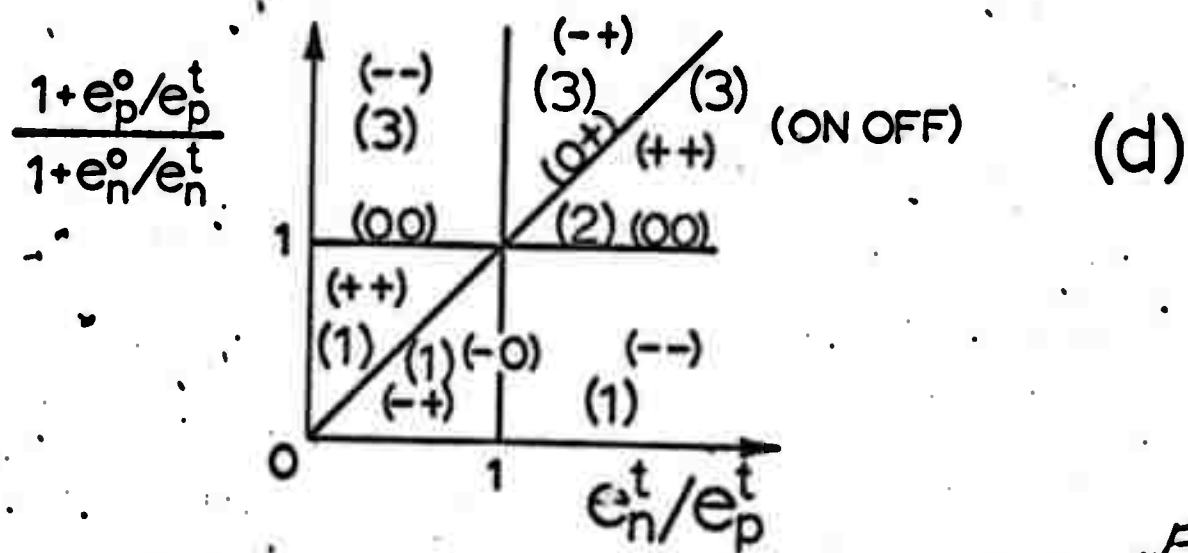
(a)



(b).



(c)



(d)

Fig. 4
Sah: ntr.

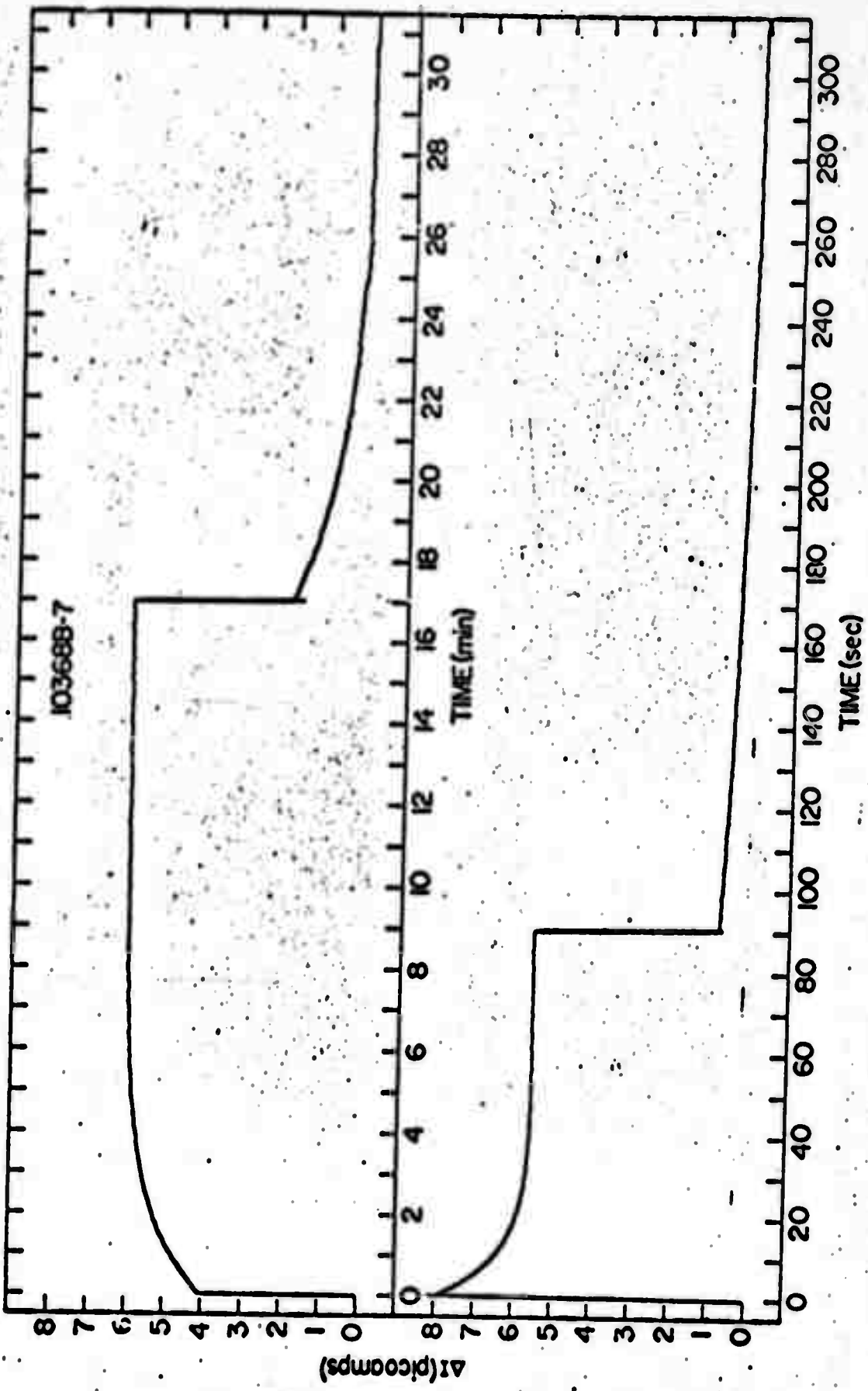


Figure 5. Examples of the experimental results. (a) Actual experimental curves recorded by the strip chart recorder.

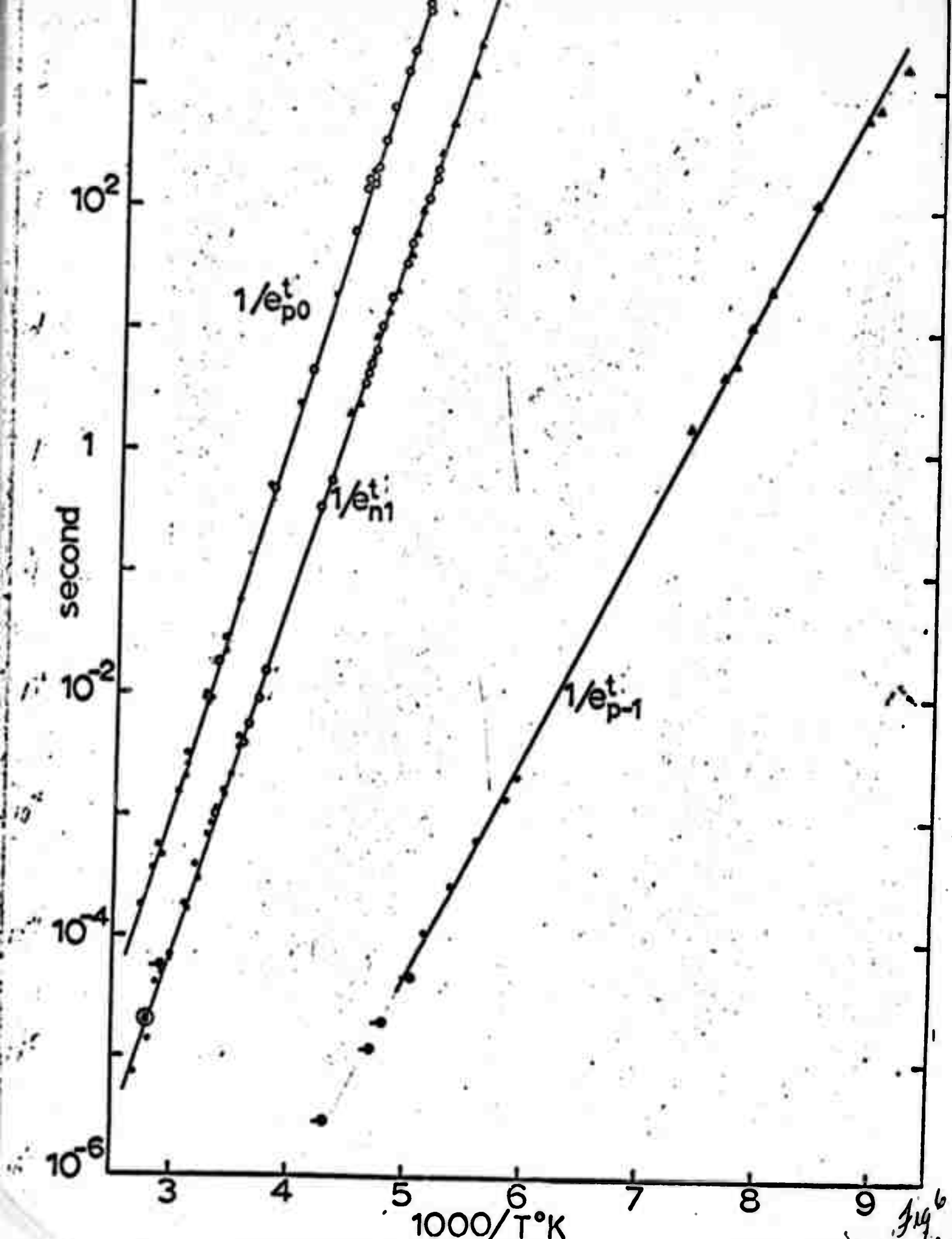


Fig. 6

